Michelson Interferometer

Duncan Beauch with Charlotte Hoelzl
October 27, 2021

I. Introduction

The Michelson-Morley experiment was a famous experiment performed in 1887 to find proof of the mysterious “aether”, the proposed medium through which light travels. The though here was that light had a preferential direction in which it would travel more quickly than another. To test this, the Michelson-Morley experiment used what is called a Michelson Interferometer to measure the speed of light in two perpendicular directions. It accomplishes this by passing the light through a beam splitter and bouncing the resulting two identical beams off a mirror the same distance away, which return to the same point. From experiments in diffraction and interference, we know that light can interfere with itself and result in complicated interference patterns which we have equations to describe. Thus, if there is a preferential direction in the “aether”, it would be observed as an interference pattern on the interferometer because the distance traveled by the two beams would be different. This experiment instead proved the opposite because as the light is sent into the interferometer it is shown to travel the exact same distance at the exact same speed. While the Michelson-Morley experiment is most known for its failure, the technique invented through the Michelson Interferometer is an important tool in modern physics. In the following experiments we will use a modified Michelson Interferometer as shown in Figure 1 with one fixed mirror and one moveable mirror. This moveable mirror allows us to measure the index of refraction of gasses and differences in distance on the order of a single wavelength of light.

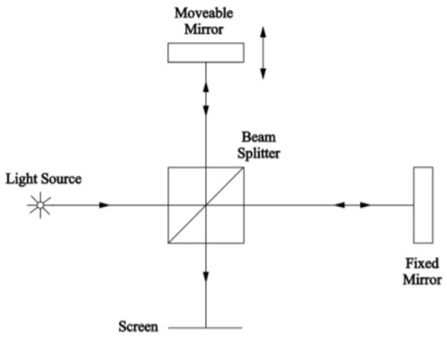

Figure 1: Michelson Interferometer with moveable mirror

II. Calibration of the Mirror Displacement Mechanism

In order to make definitive conclusions about our experiments we must make sure the interferometer is properly calibrated. The part that we are focusing here is the micrometer and lever mechanism which will be used to slide the moveable mirror. To do this, we will use a photodetector attached to the end of the interferometer where the two beams meet and create their interference pattern. This pattern will be a series of concentric circles of light intensity called fringes. We can move the mirror in and out using a 12V DC motor attached to the micrometer, allowing us to pass the fringe pattern across the photodetector. The photodetector will be used to count the fringes by plotting the intensity of light as a

$\sin^2(x)$ function where each peak in the intensity is counted as a fringe passing the photodetector. The theoretical fringe pattern is shown in Figure 2.

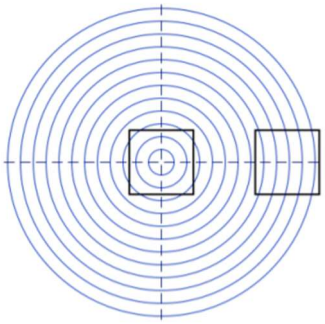

Figure 2: Fringe pattern produced by the Michelson-Interferometer

The light source used in this experiment comes from a HeNe laser with a wavelength λ = 632.8 nm. Counting the number of fringes observed over a certain distance for a pattern whose wavelength is known will allow us to calculate the precise distance traveled. Comparing this calculated number with the distance recorded by the micrometer, we can calibrate the micrometer and lever mechanism. We will begin the micrometer at a distance R_1 and use the motor and photodetector to determine the number N of fringes counted over distance R_1-R_2 where R_2 represents the final position of the micrometer.

$$R_1 - R_2 = \frac{N\lambda}{2}$$

We used the motor to count the number of fringes by starting at about R_1 = 15 mm on the micrometer and then running the motor towards the center, recording the number of fringes counted and the final position R_2 and repeating this process attempting to get the same initial and final positions ten times. We can then determine the calibration constant k, the ratio of the distance calculated to the distance recorded by the micrometer. By design, this value should be roughly 0.2 and is proven by the data collected in Table 1 where the average k value over the ten procedures was found to be k = 0.1974. However, there are several possible sources of error here. The starting and stopping would ideally be simultaneous for the motor and data requisition but since these are two different systems there is a slight delay between the two. This delay was attempted to be kept at a minimum by having the same person start and stop both devices, but introduction of human error will always be a problem. This asynchronism causes additional fringe counts to be detected as the system is very touchy and sound and movement around the detector can cause artificial fringes to be added to the

R_1	σ_{R1}	R_2	σ_{R2}	$\lvert R_1 - R_2 \rvert$	$\sigma_{R1\text{-}R2}$	N_C	σ_{NC}	D_λ	$\sigma_{D\lambda}$	k_i	σ_{ki}
mm	mm	mm	mm	mm	mm	counts	counts	mm	mm		
15.0610	0.0025	9.8250	0.0025	5.2360	0.0035	3,299	2	1.04380	0.00063	0.19935	0.00018
14.9750	0.0025	9.8100	0.0025	5.1650	0.0035	3,267	2	1.03368	0.00063	0.20013	0.00018
15.0860	0.0025	10.0080	0.0025	5.0780	0.0035	3,197	2	1.01153	0.00063	0.19920	0.00019
14.9480	0.0025	9.7210	0.0025	5.2270	0.0035	3,246	2	1.02703	0.00063	0.19649	0.00018
14.9460	0.0025	9.8590	0.0025	5.0870	0.0035	3,200	2	1.01248	0.00063	0.19903	0.00019
15.1110	0.0025	10.1060	0.0025	5.0050	0.0035	3,151	2	0.99698	0.00063	0.19920	0.00019
15.0210	0.0025	9.3790	0.0025	5.6420	0.0035	3,329	2	1.05330	0.00063	0.18669	0.00016
15.0610	0.0025	9.9890	0.0025	5.0720	0.0035	3,186	2	1.00805	0.00063	0.19875	0.00019
14.9760	0.0025	9.8490	0.0025	5.1270	0.0035	3,206	2	1.01438	0.00063	0.19785	0.00018
15.1610	0.0025	10.0230	0.0025	5.1380	0.0035	3,210	2	1.01564	0.00063	0.19767	0.00018

Table 1: Data recorded through the fringe-counting process described

total count. Additionally, the lights in the room being on affect the intensity measured by the detector which add an uncertainty to the fringe count. We had to close the blinds on the window behind our interferometer in an attempt to minimize this. Ideally this experiment would be done in a dark room with no other light sources, but it has been found through repeated experiments that the results are close enough with the lights on.

III. Measurement of Index of Refraction of Air and CO2

Now we will adjust our setup to allow us to measure the index of refraction for a gas cell of first air and then CO_2. The motor and photodetector are removed from the setup as they are not needed. We now place two empty, identical glass cells of length D in each path that the light takes to ensure that the index of refraction of the glass can be ignored. As light passes through each medium, more wavelengths pass per unit distance as though it traveled further through the medium than the same distance through air. While air does have an index of refraction, this effect is irrelevant since both split beams travel through the same system. The difference will be that one gas cell is filled with a gas whose pressure we will decrease towards a near vacuum. The resulting interference pattern will be observed on a viewing screen rather than digitally recorded with a mark as a reference to keep track of the current fringe. We will purge the gas cell three times to rid any gas currently in the cell that is not air. Once the cell is filled, the pressure of the gas cell is slowly decreased using a manual vacuum pump, recording the current pressure and fringe number as they pass. This plot of pressure vs. fringe number appears as a declining straight line whose slope is $\frac{\Delta p}{\Delta N}$. This can be used to calculate the index of refraction for room-temperature air at standard atmospheric pressure:

$$n_{atm} - 1 = \frac{\lambda}{2D}(p_{atm} * \frac{\Delta N}{\Delta p})$$

Using the data collected in the procedure, the index of refraction for room-temperature air at standard atmospheric pressure was found to be $n_{air} = 267 \times 10^{-6}$. This is off by 0.7% from the accepted value of 269×10^{-6}. The plot of pressure vs. fringe index is shown in Figure 3 and corresponding least squares regression fit in Table 2.

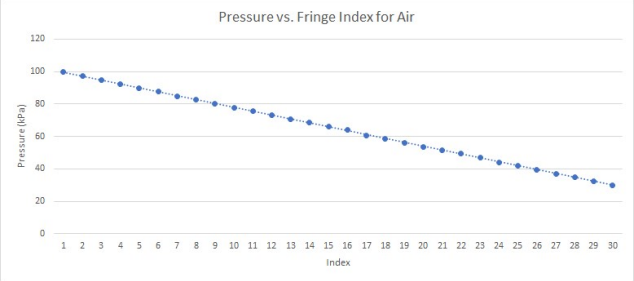

Figure 3: Pressure vs. Fringe Index for air at room-temperature and standard atmospheric pressure

	Slope	Intercept
Value	-2.39778	101.941
Error	0.004657	0.082667
Correlation	0.999894	0.220755

Table 2: Least squares regression fit for pressure vs. fringe index of air

This process can then be repeated for CO_2 to find its index of refraction. This time however, we will use a balloon filled with CO_2 to fill the gas cell rather than let air flow freely into the tube. Both the balloon and the gas cell are purged three times when filling them respectively to allow the maximum amount of gas to fill the volume. The process was repeated, and index of refraction calculated to be $n_{CO2} = 407 \times 10^{-6}$

which is off by 2.2% from the accepted value of 416 x 10^{-6}. The corresponding plot of pressure vs. fringe index and least squares regression fit can be seen in Figure 4 and Table 3 respectively.

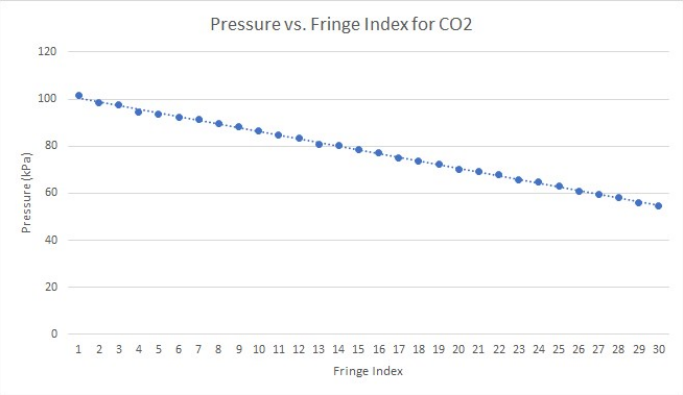

Figure 4: Pressure vs. Fringe Index for CO2 at room temperature and standard atmospheric pressure

	Slope	Intercept
Value	-1.57683	102.1539
Error	0.009406	0.166979
Correlation	0.999005	0.445904

Table 3: Least squares regression fit for pressure vs. fringe index for CO2

There are several possible sources of error for this experiment. The pump is not smooth, so it is difficult to get exactly one fringe to pass. For example, one fringe might start to the left of our marked line but the next one might start on the right, just by the nature of the jerky movements of the pump. The vacuum pump was much more sensitive for CO_2 than for air which made accurate measurements of the fringe index more difficult which explains why the graph is slightly more erratic than the graph for air. Fringes passed much quicker for CO_2 than for air so it was difficult to get precisely one fringe to pass when pumping air out.

IV. Measurement of the Wavelength Difference for Sodium D lines

Now we replace the HeNe laser with a sodium lamp with $\lambda = 589.29$ nm. The lamp is placed as close to the entrance to the interferometer as possible with a glass diffusing plate installed in between. Rather than viewing the interference pattern on a viewing screen, we will look directly into the exit aperture. The resulting pattern transitions from series of fuzziness to bright multi-colored fringes as the micrometer is adjusted with the pattern repeating every thousand fringes. We can calculate the difference between the two spectral lines of the sodium lamp using the number of fringes N passed over the distance d_{fuzzy} between fuzziness and clear fringe patterns. d_{fuzzy} can be calculated using the average measured distances between three periods of fuzziness and sharp fringes, multiplied by our calibration constant k found in experiment 1.

$$d_{fuzzy} = \frac{\Delta d}{3} * k$$

$$N_i = \frac{2d_{fuzzy}}{\lambda_i} \qquad N_1 = N_2 + 1$$

Rearranging these equations and assuming $\lambda_1 \approx \lambda_2$, we find that the difference between the spectral lines:

$$\Delta\lambda = \frac{\lambda^2}{2d_{fuzzy}}$$

Using measurements found experimentally, we find that $\Delta\lambda = 0.5946$ nm which is off by 0.4% from the expected value 0.597 nm. There were a couple approximations made in this calculation

which can result in some errors. The number of cycles per period was estimated to be 1000 and the exact point of maximum fuzziness is quite difficult to determine. Therefore, three cycles were measured to find the value of d_{fuzzy}.

V. Zero-Path Difference and White Light Fringes

We can very precisely measure the difference in length for the two optical path lengths created by the interferometer. When the distances are the same within one wavelength of the specified light, the resulting interference pattern appears as bright white light fringes. This phenomenon was measured to happen at R = 14.374 ± 0.0025 mm. This is a significant occurrence because it tells us that the distance optical path difference is equivalent to the degree of one micrometer.

VI. Conclusion

Throughout these sets of experiments, we have found many intriguing uses of the Michelson Interferometer. In experiment 1 we showed that this tool can be calibrated rather simply by counting light fringes in the interference pattern. This calibration was then used in experiment 3 to determine the wavelength difference in the two-line spectra produced by a light source. In experiment 2 we showed that the precision of our interferometer can even be used for measuring an index of refraction for a material such as CO_2. Finally in experiment 4 we showed one of the most important uses for an interferometer, measuring optical path difference. While our setup here is rather small and has many sources of error, a larger and more precise system can be made for important experiments. The most famous of which is the experiments conducted at LIGO and VIRGO that were the first detection of gravitational waves, confirming a hypothesis of Einstein's Theory of General Relativity. In order to explore the possibilities and mysteries of physics, we need advanced measurement devices such as the interferometer to further our pursuit of knowledge.